SLAC-PUB-7778
April 1998

Influence of Miscut on Crystal Truncation Rod Scattering

A. Munkholm and S. Brennan

Submitted to *Journal of Applied Crystallography*

Stanford Linear Accelerator Center, Stanford University, Stanford, CA 94309

Work supported by Department of Energy contract DE–AC03–76SF00515.

Influence of Miscut on Crystal Truncation Rod Scattering

A. Munkholm† and S. Brennan

Stanford Synchrotron Radiation Laboratory,

Stanford Linear Accelerator Center, Stanford, CA 94309

Abstract

X rays can be used to measure the roughness of a surface by studying Crystal Truncation Rod scattering. It is shown that for a simple cubic lattice the presence of a miscut surface with a regular step array has no effect on the scattered intensity of a single rod and that a distribution of terrace widths on the surface is shown to have the same effect as adding roughness to the surface. For a perfect crystal without miscut, the scattered intensity is the sum of the intensity from all the rods with the same in-plane momentum transfer. For all real crystals the scattered intensity is better described as that from a single rod. It is shown that data collection strategies must correctly account for the sample miscut or there is a potential for improperly measuring the rod intensity. This can result in an asymmetry in the rod intensity above and below the Bragg peak, which can be misinterpreted as being due to a relaxation of the surface. The calculations presented here are compared with data taken for silicon(001) wafers with 0.1 and 4 degree miscuts.

† Current address: Materials Science Division, Argonne National Laboratory, Argonne, IL 60439

I. INTRODUCTION

In the last decade Crystal Truncation Rod (CTR) scattering has proved to be a powerful technique for investigating surface and interface structures. Significant results have been reported on surface reconstruction, relaxation and roughness by measuring the intensity distribution of the CTR [1–6]. CTR's arise from the termination of the crystal lattice at a surface or interface. The phenomenon can be thought of as a relaxation of the diffraction condition in the direction perpendicular to the surface, so that the points of scattered intensity in reciprocal space representing an infinite crystal become rods of intensity in the direction of the surface normal. These rods carry information about the termination of the crystal and an analysis of the rod profile can therefore lead to structural information of the surface or interface.

There has been a wide range of theoretical and experimental work on specular and diffuse [7–9] and grazing incidence x-ray scattering [10–12] from stepped surfaces and multilayers. The effect of miscut has also been studied using electron diffraction for vicinal silicon (001) surfaces [13]. Monte Carlo simulations of the step distribution for surfaces in thermal equilibrium have been performed to aid the interpretation of diffraction data [14]. Andrews & Cowley [15] showed experimentally that the CTR linked the Bragg reflection to the surface for both nominally oriented and miscut crystals. They explained their results using a Fourier transform description of the electron density. Robinson [16] used an atomistic approach to present the theory of crystal truncation rod scattering, but did not address the issue of miscut crystals. While it is clear that the Fourier transform and atomistic approaches give identical results for surfaces with no miscut, the effect of miscut on the decay of the crystal truncation rod intensity for a rough surface has not previously been explored for either approach.

In this paper we present theoretical calculations which compare the effect of miscut on CTR intensities for smooth and rough surfaces using both Fourier transform and atomistic approaches. These calculations are compared with data taken for silicon (001) wafers with

0.1 and 4 degree miscuts. Calculations are presented both for a simple cubic lattice and for a diamond cubic lattice. They show that the decay of intensity for a single CTR of a simple cubic lattice is unchanged by the rotation of the rod due to miscut. It is also shown that fluctuations in terrace width on a miscut surface decrease the CTR intensity in a manner consistent with roughness.

Silicon(001) wafers typically have a miscut of 0.1 degree, which for an ordered step array with single layer steps corresponds to terraces of $\sim$ 780 Å. Even this small a miscut has an influence on the direction of the CTR. As discussed above, the rod is perpendicular to the surface, so if there is a miscut, no matter how small, the CTR does not follow the principal crystallographic direction, but tilts in such a way that it is perpendicular to the surface. The separation between rods at the surface has been observed with grazing incidence x-ray scattering and used to evaluate the step distribution of a silicon (001) surface [20].

As will be shown below, dealing with miscut crystals requires special diligence in tracking the position of the rod in reciprocal space. If not done properly, one possible result is an asymmetry of the rod below and above the Bragg position. The CTR from a surface with a relaxation or reconstruction is modified from that of a bulk-terminated surface, as has been pointed out previously [1,2]. For instance, relaxation of the surface results in an asymmetry in the shape of the CTR on either side of Bragg peaks. However, there has been no evidence that oxide-terminated silicon surfaces show either a reconstruction or relaxation [17–19]. We therefore developed data collection strategies to ensure that the rod is measured correctly at each position in reciprocal space. Even for a wafer with a 0.1 degree miscut the tilt between the rods and the crystallographic axis is large enough to cause a asymmetry in the rod intensity unless the rod position is correctly determined.

II. THEORY

A. Continuum Model

A crystal with a perfectly flat surface can be described in terms of an infinite lattice multiplied by a shape function which is unity where the crystal exists and zero elsewhere. Using this model, Andrews & Cowley [15] showed that the intensity for a semi-infinite crystal is given by:

$$I \propto \sum_{\vec{\tau}} \frac{\left|\rho_0(\vec{\tau})\right|^2}{q_\perp^2} \tag{1}$$

where ρ_0 is the average electron density of the crystal. Let $\vec{Q}$ be the total scattering vector and $\vec{q}$ the momentum transfer relative to the Bragg reflection $\vec{\tau}$ ($\vec{Q} = \vec{\tau} + \vec{q}$). Then $\vec{q}_\perp$ corresponds to the reduced scattering vector, which is the momentum transfer of the Bragg reflection perpendicular to the surface. Thus rods of intensity with a $1/q_\perp^2$ dependence in the direction of the surface normal are associated with each Bragg peak in reciprocal space. For a crystal surface exactly along a crystallographic direction, rods from Bragg peaks with identical in-plane momentum transfer overlap, e.g. for the case of silicon (001), the $20\bar{2}$, 202, 206 etc. rods, the resulting CTR intensity is given by the sum over those individual rods.

The presence of a miscut will rotate the shape function with respect to the crystallographic axes, so that the Heaviside function (in the case of a perfectly flat surface) is in the direction of the surface normal. A Fourier transform of such a system is equivalent to a convolution of the reciprocal lattice with that of the Fourier transform of the Heaviside function. Since the Heaviside function is in the direction of the surface normal, so will its Fourier transform. Thus, the rods associated with each Bragg peak are rotated with respect to the crystallographic axes to be normal to the surface of the crystal. Rods from Bragg peaks with the same in-plane (crystallographic) momentum transfer remain parallel, but they no longer overlap. The intensity along the CTR is therefore not given by the sum over all the rods, but directly by the intensity from the rod arising from the Bragg peak being probed:

$$I \propto \frac{|\rho_0(\vec{\tau})|^2}{q_\perp^2} \tag{2}$$

Munkholm *et al.* [6] have shown that the intensity contribution from higher order rods to the total CTR intensity is negligible when the surface is not perfectly flat, since surface roughness causes the rod intensity to decrease exponentially as a function of $q_\perp$. If the surface is just slightly rough (rms roughness > 0.5 Å), then even for a crystal with zero miscut, the total CTR intensity is dominated by the intensity of the rod associated with the nearest Bragg peak. Thus for any real crystal having either roughness or miscut, the CTR scattering is better described as $1/q_\perp^2$ than as $\sum 1/q_\perp^2$, unless the resolution function is large compared to the splitting between the rods (i.e. small miscut angle).

B. Atomistic Model

1. No miscut

An atomistic approach was used by Robinson in which the structure factor is summed up for each atomic layer of crystal to yield the crystal truncation rod intensity [16]. The theory was presented for a simple tetragonal lattice, and is reproduced here for a simple cubic lattice. For a simple cubic lattice with a perfectly flat surface, the structure factor can be expressed as:

$$F(\vec{Q}) = f_0 \sum_{j_1=1}^{N_1} \sum_{j_2=1}^{N_2} \sum_{j_3=1}^{N_3} e^{i(Q_1 a_1 j_1 + Q_2 a_2 j_2 + Q_3 a_3 j_3)} \tag{3}$$

$$= f_0 \left(\frac{e^{iQ_1 a_1 N_1} - 1}{e^{iQ_1 a_1} - 1} \right) \left(\frac{e^{iQ_2 a_2 N_2} - 1}{e^{iQ_2 a_2} - 1} \right) \left(\frac{e^{iQ_3 a_3 N_3} - 1}{e^{iQ_3 a_3} - 1} \right) \tag{4}$$

where f_0 is the atomic form factor, $\vec{Q}$ is the scattering vector and the subscript numbers refer to the projection of $\vec{Q}$ onto the crystal axis. N_1, N_2 and N_3 correspond to the number of unit cells in the crystal along these three directions. Replacing the scattering vector representation with its reciprocal space equivalent ($Q_1 a_1 = 2\pi h$, $Q_2 a_2 = 2\pi k$, $Q_3 a_3 = 2\pi l$) yields:

$$F(h,k,l) = f_0 \left(\frac{e^{2\pi i h N_1} - 1}{e^{2\pi i h} - 1}\right)\left(\frac{e^{2\pi i k N_2} - 1}{e^{2\pi i k} - 1}\right)\left(\frac{e^{2\pi i l N_3} - 1}{e^{2\pi i l} - 1}\right) \tag{5}$$

The intensity is thus given by:

$$\begin{aligned} I &= F(h,k,l)F^*(h,k,l) \\ &= |f_0|^2 \left(\frac{\sin^2(\pi h N_1)}{\sin^2(\pi h)}\right)\left(\frac{\sin^2(\pi k N_2)}{\sin^2(\pi k)}\right)\left(\frac{\sin^2(\pi l N_3)}{\sin^2(\pi l)}\right) \end{aligned} \tag{6}$$

At the integer position of h and k the intensity from the two first products is equal to $N_1^2 N_2^2$. The introduction of a surface on the crystal corresponds to a relaxation of the diffraction condition in the direction of the surface normal [16]. Thus, for a semi-infinite crystal with a surface perpendicular to the [001] direction, the intensity is:

$$I = |f_0|^2 N_1^2 N_2^2 \frac{1}{2\sin^2(\pi l)} \qquad h, k = integer \tag{7}$$

2. Miscut

To see the effect of miscut on the formalism reproduced above, it is clearest to demonstrate for a simple cubic lattice. In Appendix A we develop the more complicated (and more useful) case of a diamond cubic lattice. Consider a simple cubic lattice with a miscut m in the [100] direction as shown in Figure 1 with a regular array of terraces (the width of all the terraces are the same). Let the miscut crystal be terminated by N_t terraces each consisting of M unit cells in the miscut direction. Thus the crystal has $N_1 = MN_t$ unit cells in the [100] direction, N_2 unit cells in the [010] direction and N_3 unit cells in the [001] direction. It is convenient to describe the step array as a stacking of planes which are perpendicular to the [100] direction. The structure factor for a single plane is:

$$F_{plane} = f_0 \sum_{j_2=0}^{N_2-1} e^{2\pi i k j_2} \sum_{j_3=0}^{N_3-1} e^{2\pi i l j_2} = f_0 \left(\frac{e^{2\pi i k N_2} - 1}{e^{2\pi i k} - 1}\right)\left(\frac{e^{2\pi i l N_3} - 1}{e^{2\pi i l} - 1}\right). \tag{8}$$

The structure factor for the whole crystal is given by summing over the planes of a terrace, then over all the terraces. Because it is a simple cubic lattice, the translation vector from the end of one terrace to the beginning of the next $\vec{t}$ is given by $[10\bar{1}]$.

$$F = F_{plane} \sum_{j_1=0}^{M-1} e^{2\pi i h j_1} \sum_{j_s=0}^{N_t-1} e^{2\pi i (Mh-l) j_s}$$
$$= f_0 \left(\frac{e^{2\pi i k N_2} - 1}{e^{2\pi i k} - 1} \right) \left(\frac{e^{2\pi i l N_3} - 1}{e^{2\pi i l} - 1} \right) \left(\frac{e^{2\pi i h M} - 1}{e^{2\pi i h} - 1} \right) \left(\frac{e^{2\pi i (Mh-l) N_t} - 1}{e^{2\pi i (Mh-l)} - 1} \right) \quad (9)$$

The scattered intensity is given by:

$$I = |f_0|^2 \left(\frac{\sin^2(\pi k N_2)}{\sin^2(\pi k)} \right) \left(\frac{\sin^2(\pi l N_3)}{\sin^2(\pi l)} \right) \left(\frac{\sin^2(\pi h M)}{\sin^2(\pi h)} \right) \left(\frac{\sin^2(\pi (Mh-l) N_t)}{\sin^2(\pi (Mh-l))} \right) \quad (10)$$

The first two products in the above equation are equivalent to those derived for a perfect crystal with no miscut. The first product is a sum over the atoms in the k-direction, which for an infinite array yields a delta-function for any integer of k. The second product is a sum in the l-direction, which, because N_3 is finite, results in a decay of the scattering away from the Bragg reflection in the [001] direction. The third product arises from summing over the atoms on each terrace and causes peaks at the integer positions in the [100] direction. Because M is relatively small, the envelope function in the h-direction is larger than in k or l. The larger the terraces (the smaller the miscut) the sharper these peaks are.

In equation 10 the last product determines the tilt of the rod, i.e. the h and l values where the maximum intensity occurs. For the rod going through the Bragg reflection HKL, h is for a given terrace width M given by:

$$h = H + \frac{l - L}{M} \quad (11)$$

or

$$l = M(h - H) + L \quad (12)$$

M is the slope of the rod, and when $h = H$, $l = L$. Because we are dealing with a simple cubic cell, $-1/M$ is the slope of the surface, 1 cell down for each M cells across. Thus the rod is perpendicular to the surface.

Inserting equation 11 into equation 10 gives the intensity along the rod as a function of l only:

$$I_{ctr} = |f_0|^2 N_t^2 N_2^2 \left(\frac{\sin^2(\pi l N_3)}{\sin^2(\pi l)}\right)\left(\frac{\sin^2(\pi(HM+l-L))}{\sin^2(\pi(H+(l-L)/M))}\right) \tag{13}$$

since M, H and L are all integers, the equation can be further simplified to:

$$I_{ctr} = |f_0|^2 N_2^2 N_t^2 \left(\frac{1}{2\sin^2(\pi l)}\right)\left(\frac{\sin^2(\pi l)}{\sin^2(\pi(l-L)/M)}\right) = \frac{|f_0|^2 N_2^2 N_t^2}{2\sin^2(\pi(l-L)/M)} \tag{14}$$

Since $\sin^2(x)$ can be approximated as x^2 for small values of x, then the rod profile can be written as:

$$I_{ctr} = |f_0|^2 \frac{N_2^2 N_t^2 M^2}{2\pi^2(l-L)^2} \tag{15}$$

Thus the atomistic approach reaches the same conclusion that was reached by the continuum model, that the CTR intensity from a stepped surface is that from each rod separately, rather than the sum over all the rods, as would be the case for a surface along the crystallographic direction.

The influence of a variation of terrace length on the CTR intensity can be studied by examining the scattering from a step array with a period of two terraces of width M_1 and M_2 unit cells, respectively. For a crystal consisting of N_t terraces with $2M$ unit cells per bi-terrace ($2M = M_1 + M_2$) the structure factor is:

$$\begin{aligned} F &= F_{plane}\left(\sum_{j_1=0}^{M_1-1} e^{2\pi i h j_1} + e^{2\pi i(hM_1-l)}\sum_{j_2=0}^{M_2-1} e^{2\pi i h j_2}\right)\sum_{j_s=0}^{N_t/2-1} e^{2\pi i(2Mh-2l)j_s} \\ &= F_{plane}\left(\left(\frac{e^{2\pi i h M_1}-1}{e^{2\pi i h}-1}\right) + e^{2\pi i(hM_1-l)}\left(\frac{e^{2\pi i h M_2}-1}{e^{2\pi i h}-1}\right)\right)\left(\frac{e^{2\pi i(Mh-l)N_t}-1}{e^{4\pi i(Mh-l)}-1}\right) \end{aligned} \tag{16}$$

The step height is assumed to be one unit cell as in the case of the regular step array. The intensity is then given by:

$$I = |f_0|^2 \left(\frac{\sin^2(\pi k N_2)}{\sin^2(\pi k)}\right)\left(\frac{\sin^2(\pi l N_3)}{\sin^2(\pi l)}\right)\left(\frac{I_{bracket}}{4\sin^2(\pi h)}\right)\left(\frac{\sin^2(\pi(Mh-l)N_t)}{\sin^2(2\pi(Mh-l)}\right) \tag{17}$$

where

$$
\begin{aligned}
I_{bracket} &= \left(e^{2\pi i M_1 h} - 1 + e^{2\pi i(2Mh-l)} - e^{2\pi i(M_1 h - l)}\right) \cdot ComplexConjugate \\
&= 4 - 2\cos(2\pi M_1 h) - 2\cos(2\pi M_2 h) - 2\cos(2\pi(2Mh-l)) - \\
&\quad 2\cos(2\pi l) + 2\cos(2\pi(M_1 h - l)) + 2\cos(2\pi(M_2 h - l)) \\
&= 4\Big(\sin^2(\pi M_1 h) + \sin^2(\pi M_2 h) + \sin^2(\pi(2Mh-l)) + \\
&\quad \sin^2(\pi l) - \sin^2(\pi(M_1 h - l)) - \sin^2(\pi(M_2 h - l))\Big)
\end{aligned} \tag{18}
$$

The first, second and last products in equation 17 are identical to that of a regular step array (see equation 10). Therefore the rod is oriented in the direction perpendicular to the surface of the crystal as expected. As in the case of a regular step array, the intensity along the rod can be examined by inserting the following condition on h, where HKL is the Bragg reflection associated with the rod.

$$
h = H + \frac{2(l-L)}{M_1 + M_2} = H + \frac{(l-L)}{M} \tag{19}
$$

Note the similarity between equation 19 and 11, where M in the equation above corresponds to average terrace width, whereas M in equation 11 is the exact terrace width. Thus, the rod intensity as a function of l for a bi-terrace structure is given by:

$$
\begin{aligned}
I_{ctr}^{2step} = |f_0|^2 N_t^2 &\left(\frac{\sin^2(\pi k N_2)}{\sin^2(\pi k)}\right)\left(\frac{\sin^2(\pi l N_3)}{\sin^2(\pi l)}\right)\left(\frac{1}{\sin^2(\pi(H + (l-L)/M))}\right)\cdot \\
&\Big(\sin^2(\pi(HM_1 + (l-L)\frac{M_1}{M})) + \sin^2(\pi(HM_2 + (l-L)\frac{M_2}{M})) + \\
&\sin^2(\pi(2HM + l - 2L)) + \sin^2(\pi l) - \\
&\sin^2(\pi(HM_1 + (l-L)\frac{M_1}{M} - l)) - \sin^2(\pi(HM_2 + (l-L)\frac{M_2}{M} - l))\Big)
\end{aligned} \tag{20}
$$

since M_1, M_2, M, H and L are all integers, the equation can be written as:

$$
\begin{aligned}
I_{ctr}^{2step} = |f_0|^2 N_t^2 N_2^2 &\left(\frac{1}{4\sin^2(\pi l)}\right)\left(\frac{1}{\sin^2(\pi(l-L)/M)}\right)\Big(\sin^2(2\pi(l-L)\frac{M_1}{M}) + \\
&\sin^2(2\pi(l-L)\frac{M_2}{M}) + 2\sin^2(\pi l) - \sin^2(\pi(2(l-L)\frac{M_1}{M} - l)) - \\
&\sin^2(\pi(2(l-L)\frac{M_2}{M} - l))\Big)
\end{aligned} \tag{21}
$$

In the limit of a perfect step array $M_1 = M_2 = M$, the products which contain either M_1 or M_2 drop out of equation 21 and it reduces to equation 14, which is the rod intensity for a regular step array. However if M_1 is not equal to M_2 a decrease in the intensity occurs. This is shown in Figure 2, where the CTR intensity is plotted for different terrace width combinations. All the curves shown correspond to the same miscut of 0.57 degree $(M_1 + M_2 = 100)$. For a regular step array $(M_1 = M_2)$ the fall off goes as $1/q^2$, however as the difference in terrace width increases, the intensity drops faster, i.e. the surface is rougher. Note that the effect of varying the terrace width on scattered intensity has been observed in the specular reflectivity of the (000) rod for multilayers grown on miscut surfaces [8]. The distribution in terrace widths results in an increase in diffuse scattering which can be observed at h and k values separated from the CTR. Depending on the resolution function of the experiment that scattering will either be collected by the detector or not [6].

Appendix A is the derivation of the scattered intensity from a regular step array on the surface of the diamond cubic lattice of silicon. The intensity is:

$$I_{ctr} = 4|f_0|^2 \cos^2(\frac{\pi}{4}(2H + (4M_1 + 2)\frac{l - L}{M_{tot}} - l)) \cos^2(\frac{\pi}{2}(M_{tot}H + K - L))\frac{N_2^2 N_t^2 M_{tot}^2}{2\pi^2(l - L)^2}. \quad (22)$$

The difference between this equation and the equation for the diamond cubic surface without miscut is the term $(4M_1 + 2)(l - L)/M_{tot}$ in the first $cos^2()$. If $(4M_1 + 2) = M_{tot}$ then the scattered intensity is that of a surface without miscut. If they are not equal, then the reduction in intensity observed for the simple cubic case is observed here.

III. ROD POSITION

Due to the extended nature of the CTR one cannot find the maximum of the rod at a particular l-value by using the same approach employed to locate a Bragg peak. A χ-scan [21] is not orthogonal to the rod and a θ-scan is only orthogonal for small values of $\Delta\theta$, so sequentially scanning those angles will inevitably change the l-value towards that of the Bragg peak. Rather than operating in angle space and scanning single motors, one

must scan along axes in reciprocal space using multiple motors simultaneously. Consider a cubic crystal with the surface normal approximately along the [001] direction. By scanning sequentially in the h and k-direction at a constant l-value, the maximum intensity of the rod is found for that l-value, thus ensuring that the center of the rod is located for a specific out-of-plane momentum transfer away from the Bragg peak. An example of this procedure is presented in the results section below. If the size and direction of the miscut is known, the position of the rod can be calculated. However since the CTR is a very sharp feature parallel to the surface, such a calculation is only a predictor of the rod position and it is still necessary to perform the h and k-scans in order to locate it exactly. Most diffractometers have a non-zero sphere of confusion, which also limits the predictability of the rod position. Note that this problem is exacerbated by having small aperatures at the detector. For a sufficiently open detector slit, the peak of the rod will be observed by a θ-scan, but for slits set to observe long in-plane roughness correlations [6] the more complicated method described above must be used.

IV. EXPERIMENTAL

In order to investigate the influence of miscut on CTR scattering, we examined two silicon (001) wafers with different miscuts: one with a 4 degree miscut and one with a 0.1 degree miscut. The 4 degree miscut sample is terminated by an 110 Å thermal oxide, whereas the other wafer is capped by a 60 Å thermal oxide. The oxide thickness does not influence the CTR, as the CTR is unaffected by an amorphous layer. Experiments were performed at Stanford Synchrotron Radiation Laboratory (SSRL) beam lines 7-2 and 10-2 with a four-circle diffractometer using a symmetric scattering geometry (ω=0 mode) [21]. The photon energy passed by the Si(111) double crystal monochromator was selected to be 10 keV. The wafers were mounted on a vacuum chuck and kept in a helium environment to reduce air scattering. Slits were defined using the procedure of Specht and Walker [22], which uses a large diffraction-plane slit opening, allowing the entire diffracted beam to be collected by

the detector simultaneously, so that the integrated intensity is directly measured. The data were corrected for background, the Lorentz-factor, the change in atomic form factor as a function of the magnitude of the scattering vector and the area of the sample illuminated by the beam.

V. RESULTS

Figure 3 shows the intensities of the rods associated with two of the $< 202 >$ type reflections for a silicon (001) wafer with a ~ 4 degree miscut. The 202 and 022 rods are separated by a rotation of 90 degrees. In Figure 3 the plotted intensity was obtained using our traditional method of doing a single θ rocking curve at the integer position to find the maximum intensity, followed by moving to that hkl value with $\omega = 0$, then performing a θ-scan to determine the integrated rod intensity. The '+'s represent the intensity from the 202 rod and the 'o's that of the 022 rod. It has been shown [6] that the derived roughness should not depend on which rod is measured, nor should it depend on whether the rod is above or below the Bragg position. Thus all four of the rods should result in identical roughness values. The best fits to the data using the $1/q_{\perp}^2$ dependence [6] are shown as dashed and solid lines for the 202 and 022 rod, respectively. One can immediately see that the rods are asymmetric between the low and high side of the Bragg peak, and that the asymmetry flips on a rotation of 90 degrees. The derived roughness ranges from 2.3 Å to 5.8 Å.

As mentioned in the introduction, surface relaxation could have caused the asymmetry observed in Figure 3. If that were the case, however, the asymmetry would be the same for all $< 20l >$ rods, whereas for these data the asymmetry is reversed between the 202 and 022 rod. We will show instead that this asymmetry is due to our method of finding the position of the CTR using θ rocking curves.

The series of h-scans shown in Figure 4 were performed in order to locate the rod position at l=1.8 of the 022 rod. The curves represent a five-fold increase in rod intensity after

subtraction of the background. The insert in the figure shows the traces in reciprocal space of the h and k-scans performed to locate the rod position at $l = 1.8$ for the CTR associated with the 022 reflection. The horizontal lines represent the h-scans, which are the curves shown in the main part of the figure. The vertical lines correspond to the k-scans, which were done sequentially between the h-scans. The dots are placed at the maximum intensity of each scan. The CTR location at $l = 1.8$ was determined to be at h=-0.0101 and k=2.0085, which is 0.0132 rlu away from the nominal rod position corresponding to a tilt of the rod of 3.8 degrees with respect to the [001] direction. From these curves it is clear that a θ rocking curve at the integer position is not sufficient when determining the CTR intensity, as such a procedure would result in a lower rod intensity than is actually present.

In Figure 5 the intensity of the rods are shown using h and k-scans to determine the maximum of the rod at the required l-value, followed by the θ-scan as before. The best fit to each of the sides of the 202 rod both yield a roughness of 2.3 Å. Fitting the 022 rod results in a 2.3 Å rms value for the low side of the rod and 2.4 Å for the high side, which is within the estimated errorbars of $\pm$ 0.1 Å.

Although the tilt of the rod is directly proportional to the size of the miscut, one needs to be careful even for very small miscut. We have measured rods associated with both the 202 and 311 reflection for a silicon (001) wafer with a 0.1 degree miscut. Performing θ rocking curves at the integer positions leads to a nice symmetric 202 rod intensity, however, the 311 shows strong asymmetry as shown in Figure 6. A fit to the low side of the rod yields an rms roughness of 4.2 Å, whereas the rms value extracted from the high side of the rod is 1.4 Å. Locating the exact rod position using alternating h and k-scans before doing the θ-scan leads to a more symmetric rod profile (also shown in Figure 6). The fit to the low side of the rod gives an rms roughness of 2.1 Å and the fit to the high side yields 2.3 Å. The fit to both sides of the 202 rod of the same wafer (not shown) results in an rms roughness of 2.0 Å.

The relative sensitivity of the 202 and 311 rods to miscut can be explained by the instrument function of the experiment. The instrument function depends on the wavelengths

passed by the monochromator, the divergence of the beam and the angular acceptance of the detector [6]. In our experimental setup the shape of the instrument function is mainly dominated by the large angular acceptance of the detector: 8 mrad in the scattering plane and 2 mrad perpendicular to the scattering plane, which is a consequence of using the slit setting of Specht & Walker [22]. The angular acceptance results in a plane of allowed scattering vectors which is inclined with respect to the rod. This angle is equal to the incident angle α between the beam and the surface of the crystal. As the incident angle of the beam onto the sample is very small on the low side of the 311 rod, it is very easy to miss the rod. As an example, using 10 keV photons α=3.3 degrees at (3,1,0.5) so the rod and the instrument function are almost parallel.

The total width w of the CTR as measured using a θ rocking curve is a function of the horizontal angular acceptance of detector b and can be derived from equation 10 in [22] as:

$$w = \frac{b}{2}\frac{\tan\chi}{\cos\theta} \tag{23}$$

As χ decreases the rocking curve width also decreases. Figure 7 shows the width of the CTR as measured by a θ rocking curve vs. l-value for the 0.1 degree miscut wafer. The circles represent the 311 CTR data and the crosses the 202 CTR data. The solid lines are the best simultaneous fit to the data using equation 23, which corresponds to an acceptance of 3.0 mrad perpendicular to the diffraction plane. This derived angular acceptance is larger than the actual slit acceptance due to the convolution with the 2 mrad horizontal incident beam divergence. The 111 rod is also shown for comparison. The 311 rod has a very narrow rocking curve width, especially below the 311 reflection. This means that the rod is only in the diffraction condition over a very short angular range and thus it is difficult to probe the center of the rod. One should therefore be aware that even a very small miscut can influence the measured 311 CTR intensity and high precision in determining the rod position is essential for an accurate intensity measurement. The 111 rod has a broader rocking curve width, but is still difficult to properly map, especially below the Bragg peak. We have found the 202 rod to have the best combination of rocking curve width and intensity.

VI. CONCLUSIONS

We have shown that the scattering from a single rod in a simple cubic lattice does not depend on the miscut of the surface if there is a single terrace width on the surface. The introduction of a distribution of terrace widths on the surface results in a reduction in CTR intensity, consistent with the surface becoming rough. These calculations show that for a real crystal with miscut, the CTR scattering is only a function of the rod from the nearest Bragg reflection rather than from a sum over all reflections with the same in-plane momentum transfer.

For the case of the diamond cubic lattice an atomistic approach results in additional terms in the CTR intensity due to the basis of the lattice. These cosine terms are present even for a surface without miscut. The effect of miscut is to add an additional cosine term which results from their being two terraces with different surface terminations.

A scheme is presented which ensures that the exact position of the CTR is found prior to measuring the rod intensity. It was employed in measuring the rod intensity for silicon (001) wafers with miscuts of different size. Use of this method removed asymmetry of the rods which was otherwise observed, and thus resulted in a more accurate measurement of the interfacial roughness. The intersection of the instrument function with the rods determines the sensitivity of a particular rod to miscut. Since the instrument function is almost parallel with the rod associated with the 311 rod, one must determine the position of the rod very accurately even for a 0.1 degree miscut to avoid artificial asymmetry of the CTR intensity.

VII. ACKNOWLEDGMENTS

The authors thank A. Bienenstock for many fruitful discussions. The authors also thank L.-A. Files of Texas Instruments and J.P. Goodbread of Hewlett-Packard for supplying wafers. This work is supported by SSRL, which is funded by the Department of Energy, Office of Basic Energy Sciences under contract DE-AC03-76SF00515.

APPENDIX A: DIAMOND CUBIC LATTICE

1. No Miscut

Expanding the theory by Robinson discussed in section IIB to a diamond cubic lattice with an (001) termination is more easily done by using surface units rather than bulk units. The surface unit cell of the diamond cubic structure is shown in Figure 8. The unit cell in surface units is tetragonal with the same out-of-plane lattice length c as for the cubic unit cell ($c = a_0 = 5.431$ Å). The basis of the surface unit cell is rotated 45 degrees with respect to the in-plane vectors of the cubic unit cell, so that

$$[100]_{surf} = \frac{1}{2}[1\bar{1}0]_{bulk} \tag{A1}$$

$$[010]_{surf} = \frac{1}{2}[110]_{bulk} \tag{A2}$$

$$[001]_{surf} = [001]_{bulk}. \tag{A3}$$

This tetragonal unit cell has 4 atoms per cell so the volume is only half that of the cubic unit cell. The diamond cubic crystal can be described as a sum of planes of atoms which are perpendicular to the [100] direction as in the case of the simple cubic lattice. However, in the case of a diamond cubic lattice, two types of planes are present (A & B) as indicated in Figure 8. The structure factor from each bilayer (which has a basis of four atoms) is:

$$\begin{aligned} F_{DC-bilayer} &= f_0(1 + e^{2\pi i(\frac{k}{2}-\frac{l}{4})} + e^{2\pi i(\frac{h}{2}+\frac{k}{2}-\frac{l}{2})} + e^{2\pi i(\frac{h}{2}-\frac{3l}{4})}) \sum_{j_2=0}^{N_2-1} e^{2\pi ik} \sum_{j_3=0}^{N_3-1} e^{2\pi il} \\ &= f_0(1 + e^{\pi i(h+k-l)})(1 + e^{\pi i(k-\frac{l}{2})}) \left(\frac{e^{2\pi ikN_2} - 1}{e^{2\pi ik} - 1}\right) \left(\frac{e^{2\pi ilN_3} - 1}{e^{2\pi il} - 1}\right). \end{aligned} \tag{A4}$$

The structure factor of a diamond cubic crystal with a perfectly smooth surface is consequently given by summing the structure factor of the bilayers over all the bilayers present in the crystal:

$$\begin{aligned} F_{DC} &= F_{DC-bilayer} \sum_{j_1=1}^{N_1} e^{2\pi ihj_1} \\ &= f_0(1 + e^{\pi i(h+k-l)})(1 + e^{\pi i(k-\frac{l}{2})}) \left(\frac{e^{2\pi ihN_1} - 1}{e^{2\pi ih} - 1}\right) \left(\frac{e^{2\pi ikN_2} - 1}{e^{2\pi ik} - 1}\right) \left(\frac{e^{2\pi ilN_3} - 1}{e^{2\pi il} - 1}\right). \end{aligned} \tag{A5}$$

The two first products correspond to the basis of the unit cell, whereas the last three products are each a sum over the unit cells in the different crystallographic directions. The intensity from a perfectly flat crystal with a diamond cubic lattice is therefore:

$$I_{DC} = |f_0|^2 \cos^2(\frac{\pi}{2}(h+k-l)) \cos^2(\frac{\pi}{4}(2h-l)) \frac{\sin^2(\pi h N_1)}{\sin^2(\pi h)} \frac{\sin^2(\pi k N_2)}{\sin^2(\pi k)} \frac{\sin^2(\pi l N_3)}{\sin^2(\pi l)}. \quad \text{(A6)}$$

2. Miscut

For the unreconstructed surface, the termination of a diamond cubic lattice in the [001] direction can be done in two different ways. In one type the atomic bonds of the top layer will be in the [100] direction, whereas the other termination will have atomic bonds in the [010] direction. Introduction of steps onto the (001) surface will cause the surface structure orientation to alternate from terrace to terrace. For simplicity consider the case where the miscut direction is along a step direction, e.g. the [100] direction (i.e. the $[1\bar{1}0]_{bulk}$) with a step array as shown in Figure 9. Because there is a four atom basis to the unit cell, there can be four different terrace types on the surface and the repeat distance is over four terrace widths. Let the miscut crystal be terminated by N_t periods each consisting of four terraces in the [100] direction, with N_2 unit cells in the [010] direction and N_3 unit cells in the [001] direction. The width of this period is $M_{tot} = 2M_1 + 2M_2 + 1$, where M_1 and M_2 are the number of unit cells on each type of terrace. The extra unit cell arises from the translation vector from one terrace to the next. The structure factor of a single plane is given by:

$$F_{plane} = f_0 \sum_{j_2=0}^{N_2-1} e^{2\pi i k j_2} \sum_{j_3=0}^{N_3-1} e^{2\pi i l j_3} = f_0 \left(\frac{e^{2\pi i k N_2} - 1}{e^{2\pi i k} - 1} \right) \left(\frac{e^{2\pi i l N_3} - 1}{e^{2\pi i l} - 1} \right). \quad \text{(A7)}$$

A sum over all the planes of the four terraces yields:

$$F_{period} = F_{plane}(1 + e^{i\vec{q}\cdot(M_1\vec{a}_1+\vec{t}_1)} + e^{i\vec{q}\cdot((M_1+M_2)\vec{a}_1+\vec{t}_1+\vec{t}_2)} + e^{i\vec{q}\cdot((2M_1+M_2)\vec{a}_1+2\vec{t}_1+\vec{t}_2)}) \sum_{j=0}^{2M_1+2M_2} e^{i\vec{q}\cdot\vec{a}_1 j}, \quad \text{(A8)}$$

where $\vec{t}_1$ is the translation vector from the end of the first to beginning the second terrace ($\vec{t}_1 = \frac{1}{4}[20\bar{1}]$) and $\vec{t}_2$ is the translation vector from the end of the second to the start of the

third terrace ($\vec{t_2} = \frac{1}{4}[02\bar{1}]$), as shown in Figure 9. Thus, in equation A8, the unit cell of four atoms is represented by the atoms at the four step edges. A sum of this pseudo-unit cell over all the planes gives the total structure factor of the repeat unit. Evaluating the dot products in equation A8 yields:

$$\begin{aligned} F_{period} &= f_0(1 + e^{2\pi i((M_1+\frac{1}{2})h-\frac{1}{4}l)} + e^{2\pi i((M_1+M_2+\frac{1}{2})h+\frac{1}{2}k-\frac{1}{2}l)} + e^{2\pi i((2M_1+M_2+1)h+\frac{1}{2}k-\frac{3}{4}l)}) \\ &\quad \left(\frac{e^{2\pi ikN_2}-1}{e^{2\pi ik}-1}\right)\left(\frac{e^{2\pi ilN_3}-1}{e^{2\pi il}-1}\right)\left(\frac{e^{2\pi i(2M_1+2M_2+1)h}-1}{e^{2\pi ih}-1}\right) \\ &= f_0(1 + e^{2\pi i((M_1+\frac{1}{2})h-\frac{1}{4}l)})(1 + e^{2\pi i((M_1+M_2+\frac{1}{2})h+\frac{1}{2}k-\frac{1}{2}l)}) \\ &\quad \left(\frac{e^{2\pi ikN_2}-1}{e^{2\pi ik}-1}\right)\left(\frac{e^{2\pi ilN_3}-1}{e^{2\pi il}-1}\right)\left(\frac{e^{2\pi i(2M_1+2M_2+1)h}-1}{e^{2\pi ih}-1}\right). \end{aligned} \tag{A9}$$

The structure factor for the whole crystal is then determined by summing the structure factor of one period of four terraces over all the repeat units of the surface:

$$\begin{aligned} F &= F_{period} \sum_{j=0}^{N_t-1} e^{i\vec{q}\cdot((2M_1+2M_2)\vec{a}_1+2\vec{t}_1+2\vec{t}_2)j} \\ &= F_{period}\left(\frac{e^{2\pi i((2M_1+2M_2+1)h+k-l)N_t}-1}{e^{2\pi i((2M_1+2M_2+1)h+k-l)}-1}\right) \\ &= f_0(1 + e^{2\pi i((M_1+\frac{1}{2})h-\frac{1}{4}l)})(1 + e^{2\pi i((M_1+M_2+\frac{1}{2})h+\frac{1}{2}k-\frac{1}{2}l)}) \\ &\quad \left(\frac{e^{2\pi ikN_2}-1}{e^{2\pi ik}-1}\right)\left(\frac{e^{2\pi ilN_3}-1}{e^{2\pi il}-1}\right)\left(\frac{e^{2\pi iM_{tot}h}-1}{e^{2\pi ih}-1}\right)\left(\frac{e^{2\pi i(M_{tot}h+k-l)N_t}-1}{e^{2\pi i(M_{tot}h+k-l)}-1}\right). \end{aligned} \tag{A10}$$

The first two products in the above equation contain the information specific to the structure factor of the unit cell and it is these which determine whether a reflection is allowed. Note also that these are the only products which contain information about the size of the individual terraces and steps. Only the last two products contain information about the average miscut of the sample. The second to last product arises from a sum over the planes of each period and causes peaks at integer positions in the [100] direction. The last product is a sum of the scattering from all the periods N_t. This leads to rods which are perpendicular to the translation vector from one period to the next ($2(M_1+M_2)\vec{a}_1+2\vec{t}_1+2\vec{t}_2$). Consequently, the rods are always perpendicular to the surface of the crystal, since the terrace translation vector is in the plane of the surface. The scattered intensity is given by the square of the structure factor:

$$I = 4|f_0|^2 \cos^2(\frac{\pi}{4}((4M_1+2)h-l))\cos^2(\frac{\pi}{2}(M_{tot}h+k-l)) \\ *\left(\frac{\sin^2(\pi l N_3)}{\sin^2(\pi l)}\right)\left(\frac{\sin^2(\pi k N_2)}{\sin^2(\pi k)}\right)\left(\frac{\sin^2(\pi M_{tot}h)}{\sin^2(\pi h)}\right)\left(\frac{\sin^2(\pi(M_{tot}h+k-l)N_t)}{\sin^2(\pi(M_{tot}h+k-l))}\right). \quad \text{(A11)}$$

In equation A11 the last product determines the tilt of the rod, i.e. h as a function of l for the maximum intensity. For the crystal truncation rod associated with the HKL reflection, h is constrained to:

$$h = H + \frac{l-L}{M_{tot}} \quad \text{(A12)}$$

for $k = integer$. Note the similarity of this equation to equation 11, with M replaced here by M_{tot}. Inserting this condition on h into equation A11 gives the intensity along the rod as a function of l only:

$$I_{ctr} = 4|f_0|^2 \cos^2(\frac{\pi}{4}((4M_1+2)(H+\frac{l-L}{M_{tot}})-l))\cos^2(\frac{\pi}{2}(M_{tot}H+K-L)) \\ *\frac{\sin^2(\pi K N_2)}{\sin^2(\pi K)}\frac{\sin^2(\pi l N_3)}{\sin^2(\pi l)}\frac{\sin^2(\pi(H+l-L))}{\sin^2(\pi(H+(l-L)/M_{tot})}\frac{\sin^2(\pi(M_{tot}H+K-L)N_t)}{\sin^2(\pi(M_{tot}H+K-L))}. \quad \text{(A13)}$$

Since M_{tot}, H, K and L are all integers, the equation can be further simplified to:

$$I_{ctr} = 4|f_0|^2 \cos^2(\frac{\pi}{4}(2H+(4M_1+2)\frac{l-L}{M_{tot}}-l))\cos^2(\frac{\pi}{2}(M_{tot}H+K-L)) \\ *\frac{N_2^2 N_t^2}{2\sin^2(\pi(l-L)/M_{tot})}. \quad \text{(A14)}$$

Since $\sin^2(x)$ can be approximated as x^2 for small values of x, the rod profile can be written as:

$$I_{ctr} = 4|f_0|^2 \cos^2(\frac{\pi}{4}(2H+(4M_1+2)\frac{l-L}{M_{tot}}-l))\cos^2(\frac{\pi}{2}(M_{tot}H+K-L))\frac{N_2^2 N_t^2 M_{tot}^2}{2\pi^2(l-L)^2}. \quad \text{(A15)}$$

The first $cos^2()$ in equation A15 arises from a combination of the steps and the basis of the unit cell, whereas the second $cos^2()$ is only a function of the unit cell. This latter goes to zero when $H+K+L$ is an odd number, since $M_{tot} = 2M_1 + 2M_2 + 1$ is always an odd number. This corresponds to one of the conditions for destructive interference in a diamond cubic lattice. For this lattice the non-allowed reflections are given in surface units by:

$$H + K + L = 2n + 1 \qquad n = integer$$
$$2H + L = 4n + 2 \qquad n = integer. \tag{A16}$$

If $4M_1 + 2$ equals M_{tot}, i.e. the terrace width of the two types of terraces are identical, then the first product would be reduced to $\cos^2(\frac{\pi}{4}(2H - L))$, which corresponds to the second condition for destructive interference of the diamond cubic lattice.

REFERENCES

[1] I.K. Robinson, W.K. Waskiewicz and J. Bohr, Phys. Rev. Lett. **57**, 2714 (1986).

[2] R.G.v. Silfhout, J.F. v.d. Veen and C. Norris, Surf. Sci. **264**, 281 (1992).

[3] P.A. Bennett, B. DeVries and P. Eng, Phys. Rev. Lett. **69**, 2539 (1992).

[4] M.-T. Tang, K.W. Evans-Lutterodt and T. Boone, Appl. Phys. Lett. **62**, 3144 (1993).

[5] H. Reichert, P.J. Eng and I. Robinson, Phys. Rev. Lett. **74**, 2006 (1995).

[6] A. Munkholm, S. Brennan, and E.C. Carr, J. Appl. Phys. **82**, 2944 (1997).

[7] S. Pflanz, H.L. Meyerheim and E. Conrad, Phys. Rev. B **52**, 2914 (1995).

[8] V. Holy, C. Giannini and W. Stoltz, Phys. Rev. B **55**, 9960 (1997).

[9] C. Giannini, L. Tapfer and W. Stoltz, Phys. Rev. B **55**, 5276 (1997).

[10] C.S. Lent and P.I. Cohen, Surf. Sci. **139**, 121 (1984).

[11] P.R. Pukite, C.S. Lent, and P.I. Cohen, Surf. Sci. **161**, 39 (1985).

[12] G.T. Baumbach, S. Tixier and V. Holy, Phys. Rev. B **51**, 16848 (1995).

[13] D. Saloner *et al.*, J. Appl. Phys. **61**, 2884 (1987).

[14] N.C. Bartelt, T.L. Einstein, and E.D. Williams, Surf. Sci. **244**, 149 (1991).

[15] S. Andrews and R. Cowley, J. Phys. C: Solid State Phys. **18**, 6427 (1985).

[16] I. Robinson, Phys. Rev. B **33**, 3830 (1986).

[17] T. Rabedeau *et al.*, Appl. Phys. Lett. **59**, 706 (1991).

[18] T. Rabedeau *et al.*, Appl. Phys. Lett. **59**, 3422 (1991).

[19] G. Renaud *et al.*, Appl. Phys. Lett. **58**, 1044 (1991).

[20] G. Renaud, P.H. Fuoss, J. Bevk, and B.S. Freer, Phys. Rev. B **45**, 9192 (1992).

[21] W. Busing and H. Levy, Acta Cryst. **22**, 457 (1967).

[22] E. Specht and F. Walker, J. Appl. Cryst. **26**, 166 (1993).

FIGURES

FIG. 1. Schematic of a simple cubic crystal with a regular step array. The miscut is along the [100] direction of the lattice consisting of N_t terraces of M unit cells. $\vec{t}$ is the translation vector from the end of one terrace to the beginning of the next.

FIG. 2. CTR intensity for a simple cubic crystal terminated by a bi-terrace array. The width of the bi-terrace is constant at 100 unit cells ($2M = M_1 + M_2 = 100$). The curves represent the calculated intensity for different ratios of unit cells on one terrace (M_1) to the total number of unit cells on a bi-terrace ($2M = M_1 + M_2$). The solid curve corresponds to the CTR intensity of a regular step array ($M_1 = M_2 = 50$).

FIG. 3. X-ray scattering intensities ('+' and 'o') and fits for the 202 and 022 rods from a silicon (001) wafer terminated by 110 Å thermal oxide with a 4 degree miscut. The asymmetry in the rod intensities and the reversal of that asymmetry are a result of the incorrect method of determining the CTR position.

FIG. 4. Intensities for a series of h-scans through the 022 rod at l=1.8. The rod position was determined using alternate scans along the h and k-direction at a constant l-value. The insert shows the traces of the scans. The horizontal and vertical lines correspond to the h and k-scans, respectively. The maximum of each scan is identified by a large solid circle.

FIG. 5. X-ray scattering intensities ('+' and 'o') and fits for the 202 and 022 rods from a silicon (001) wafer terminated by 110 Å thermal oxide with a 4 degree miscut. h and k-scans were used to find the CTR position. The symmetric shapes indicate we have properly tracked the rod position (see text for details).

FIG. 6. The scattered intensity from a 311 rod is presented for a silicon (001) wafer terminated by a 60 Å thermal oxide with 0.1 degree miscut. The intensity obtained using our previous approach is shown as '+'s. The intensity measured with the scheme presented in this paper, is plotted as 'o's. The best fit to each side of the Bragg reflection is shown with dashes for our previous method and solid lines for the new method.

FIG. 7. The full width of the CTR obtained from θ-scans are plotted as a function of the l-value of the rod. The wafer is a silicon (001) with a 0.1 degree miscut and is terminated by a 60 Å thermal oxide. The best simultaneous fit to both rods corresponds to an acceptance of the slits of 3.0 mrad in the direction perpendicular to the scattering plane and is shown as solid lines in the figure. For comparison the 111 rod is also shown.

FIG. 8. A diagram of the surface unit cell of the diamond cubic lattice is shown on the left. As indicated with dashed lines, the surface unit cell is rotated 45 degrees with respect to the bulk unit cell. The interatomic bonds are shown as heavy lines and the outline of the unit cell is given by light lines. The surface unit cell consists of two planes (A & B) which contain two atoms each. Their configuration is outlined on the right.

FIG. 9. Figure 9 is a diagram of a step array of a diamond cubic lattice with a miscut in the $[100]_{surface}$ direction. The atomic bonds are shown as heavy lines, whereas the outline of the unit cell is shown with light lines. $\vec{t_1}$ and $\vec{t_2}$ represent the translation vectors from the end of one terrace to the beginning of the next terrace. Since there are two types of terraces, one with atomic bonds in the [100] direction and one in [010] direction, there also exist two types of translations.

Figure 1

Munkholm & Brennan

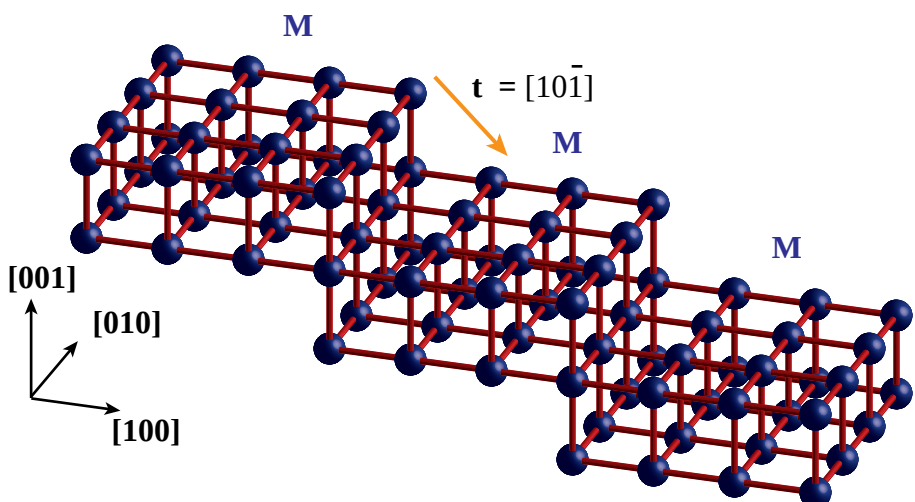

Figure 2
Munkholm & Brennan

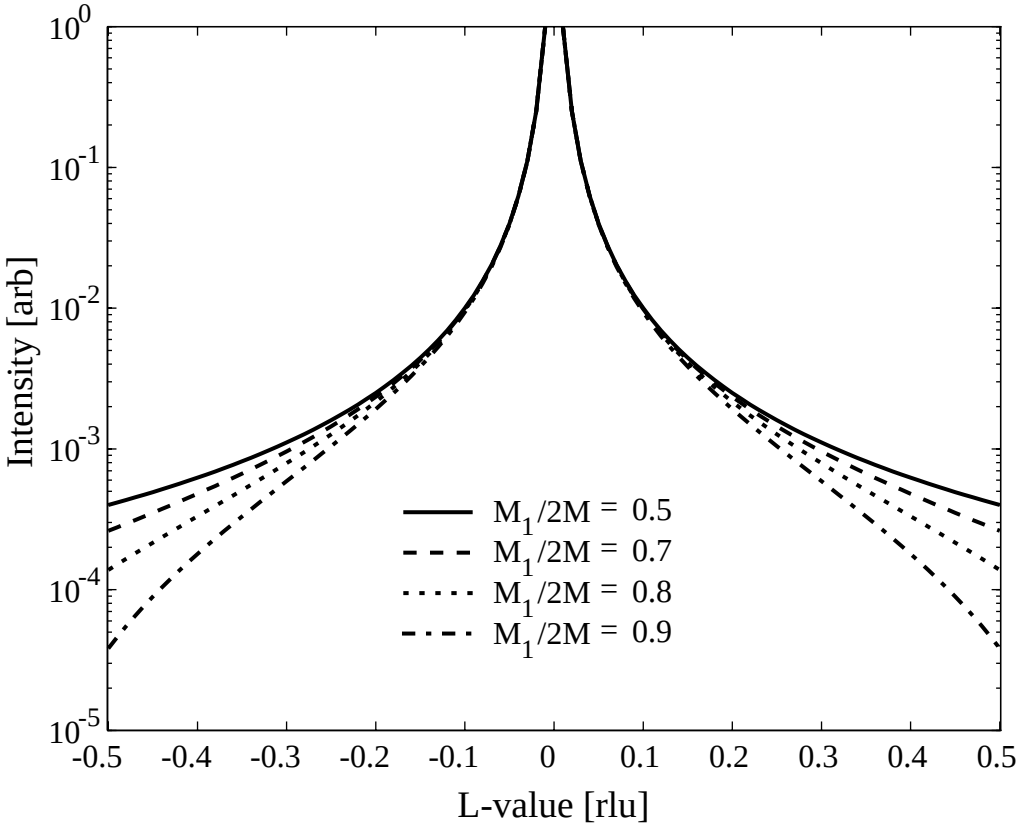

Figure 3

Munkholm & Brennan

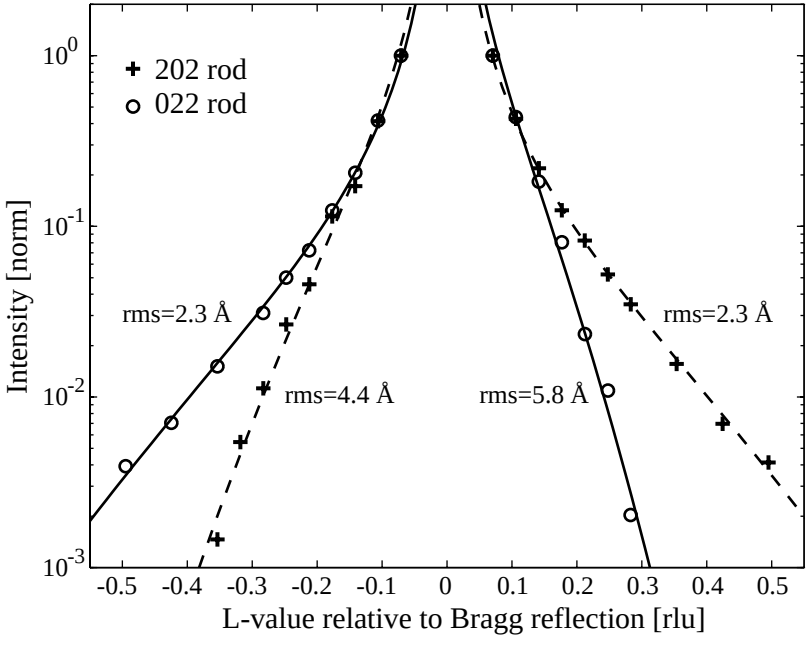

Figure 4
Munkholm & Brennan

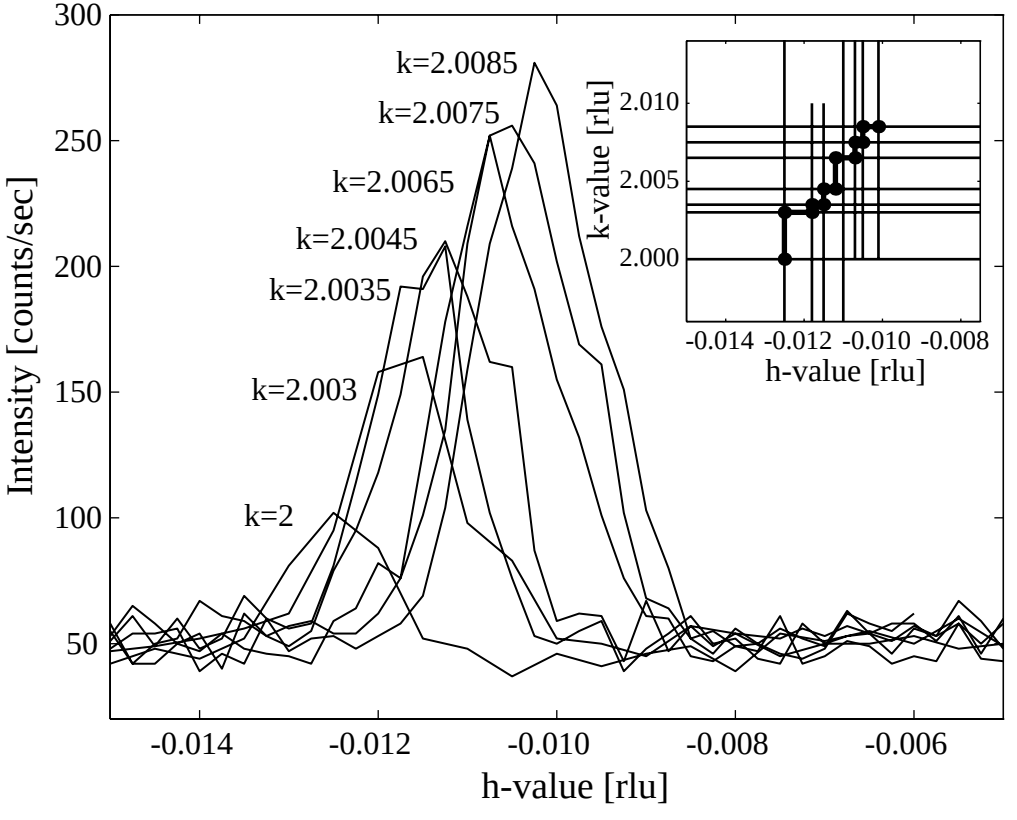

Figure 5
Munkholm & Brennan

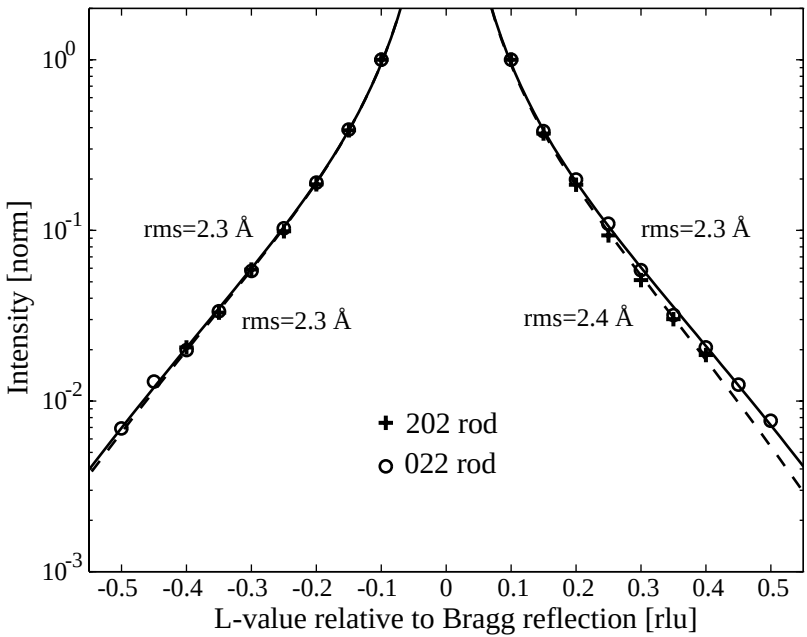

Figure 6
Munkholm & Brennan

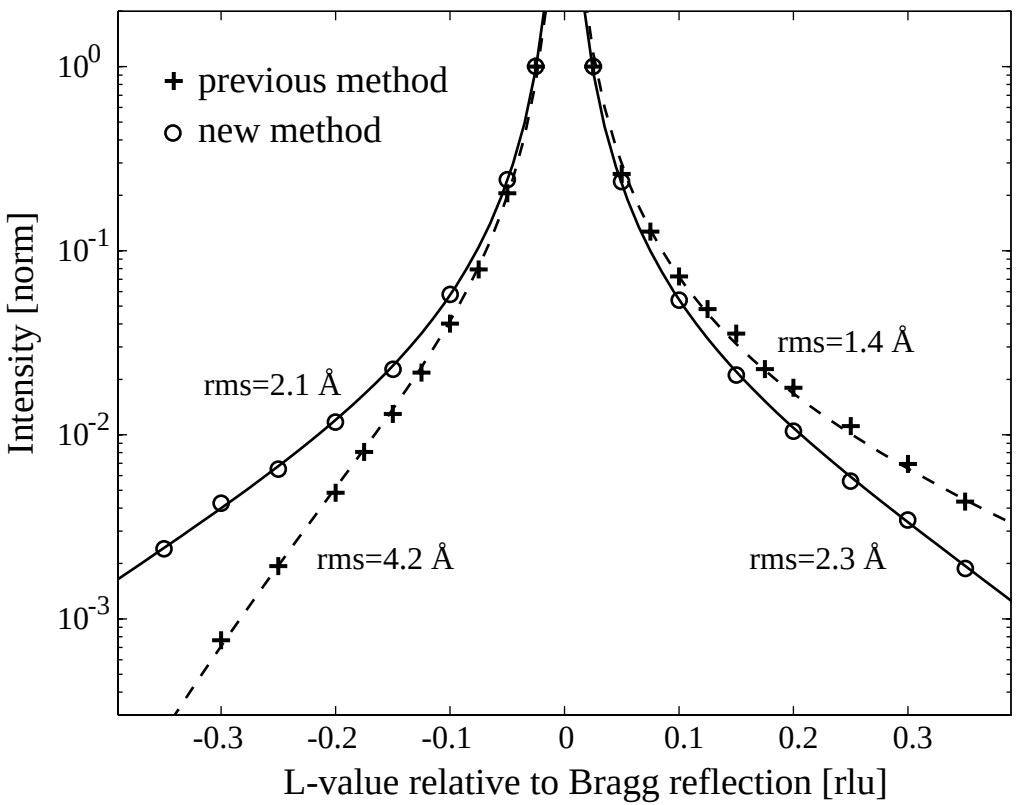

Figure 7
Munkholm & Brennan

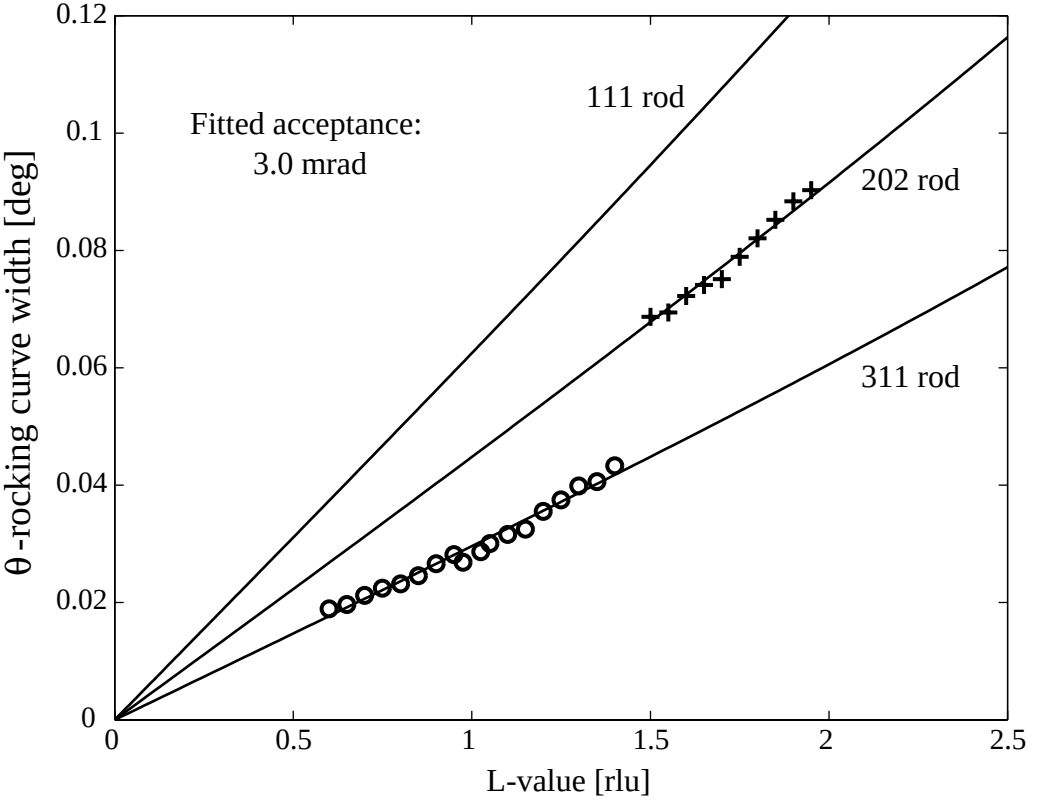

Figure 8

Munkholm & Brennan

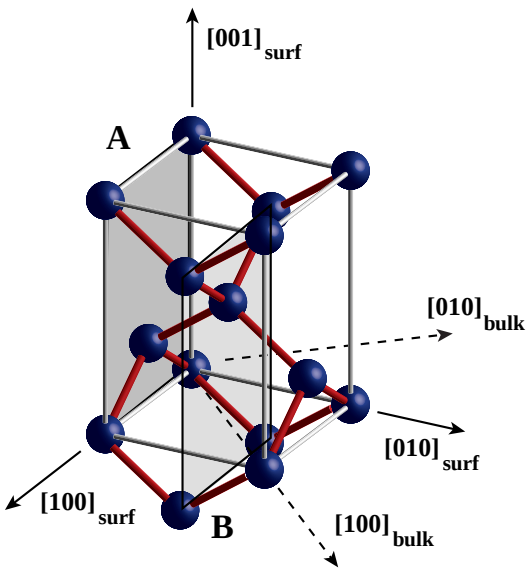

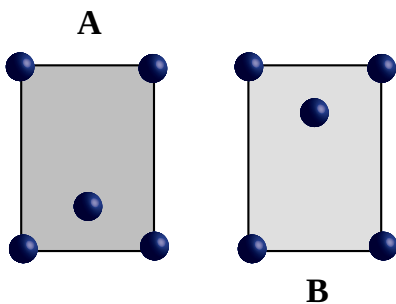

Figure 9
Munkholm & Brennan